Letters

A Novel Capacitive Coupler Array With Free-Positioning Feature for Mobile Tablet Applications

Jia-Qi Zhu, Yong-Ling Ban, Yiming Zhang, *Member, IEEE*, Chenwen Cheng, Zhengchao Yan, *Student Member, IEEE*, Rui-Min Xu, and Chunting Chris Mi, *Fellow, IEEE*

***Abstract*—This letter proposes a novel capacitive coupler array with free-positioning feature for mobile tablet applications. The capacitive coupler consists of three printed circuit boards, two of which constitute the transmitter and the third one is the receiver. The coupler is vertically arranged to make the charging system compact and feasible for mobile tablet applications. By applying a repetitive structure on the transmitter side and properly designing the receiver, free-positioning capacitive charging is realized and the coil-to-coil charging efficiency is not affected by the variation of the receiver position. Only two series inductances are utilized for compensation purposes, which makes the system more compact and easy to be fabricated. This proposed capacitive coupler is studied via finite-element analysis and verified by the experimental results at 1, 2.17, and 3.45 MHz.**

***Index Terms*—Capacitive coupler array, capacitive power transfer (CPT), free-positioning, mobile tablet application.**

I. Introduction

CAPACITIVE power transfer (CPT) utilizes electric field as media for wireless power transfer (WPT) [1]. It has three main advantages. First, proximity metallic elements do not cause significant performance degradation on CPT [2]. Second, CPT usually employs four metal plates to achieve WPT, which is very cost effective. Third, it is compact with

Manuscript received October 20, 2018; revised November 24, 2018; accepted December 5, 2018. Date of publication December 19, 2018; date of current version May 2, 2019. This work was supported in part by the National Natural Science Foundation of China under Grant 61471098, in part by the National Higher-education Institution General Research and Development Project under Grants ZYGX2016J035 and ZYGX2018J037, and in part by China Scholarship Council. *(Corresponding author: Chunting Chris Mi.)*

J.-Q. Zhu is with the School of Electronic Engineering, University of Electronic Science and Technology of China, Chengdu 611731, China, and also with the Department of Electrical and Computer Engineering, San Diego State University, San Diego, CA 92182 USA (e-mail:

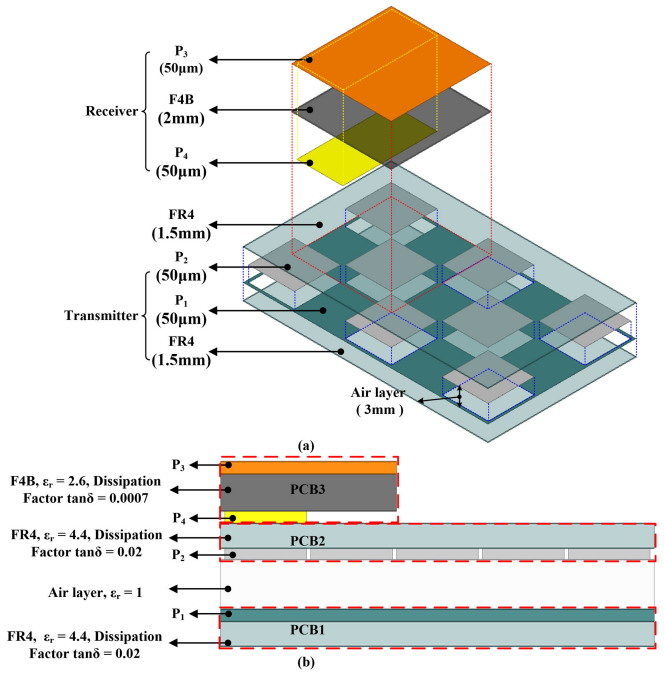

Fig. 1. (a) Breakdown diagram. (b) Side view of the proposed capacitive coupler.

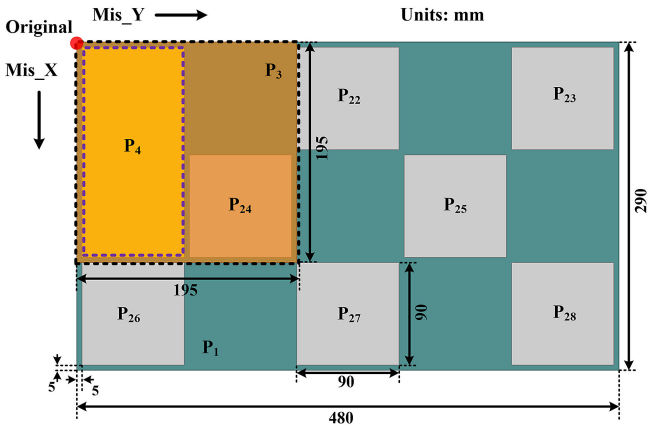

Fig. 2. Plan view of the proposed capacitive coupler.

on the top of PCB1, with an air layer gap of 3 mm. On top of the coupler is PCB3. In PCB3, the F4B dielectric layer (2 mm thickness, with relative permittivity of $\varepsilon_r = 2.6$) is sandwiched between copper plates P_3 and P_4. It is worth mentioning that PCB1 together with the air layer and the copper matrix P_2 form the transmitter. The PCB3 serves as the receiver of the system, which is supposed to be embedded inside the tablet. The FR-4 dielectric layer in PCB2 acts as the media between the transmitter and the receiver.

The plan view of the capacitive coupler is indicated in Fig. 2. Based on the dimension of an actual small desk and the IPAD PRO, the planar sizes of the transmitter and receiver are set as 480 mm × 290 mm, and 195 mm × 195 mm, respectively. At the transmitter side, the copper matrix P_2 is made up by 8 small square copper plates (P_{21}, P_{22}, ... and P_{28}) of size

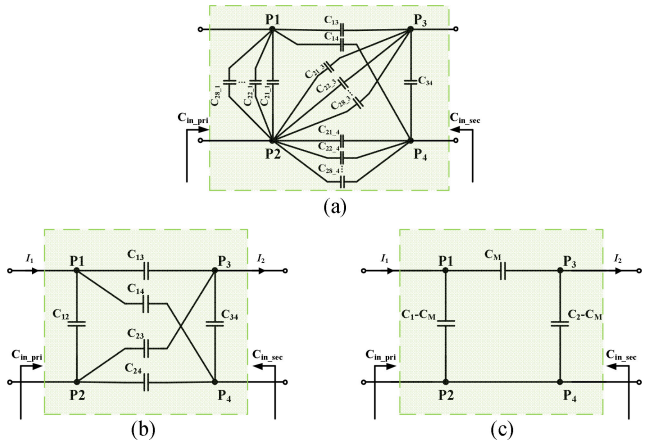

Fig. 3. (a) Circuit model of the proposed capacitive coupler. (b) Equivalent six capacitor model of the capacitive coupler. (c) Simplified π model of the capacitive coupler.

90 mm × 90 mm, which locate directly above the 8 square slots of the copper plate P_1. It needs to be pointed out that these 8 small square slots are used to decrease the self-capacitance C_1 between P_1 and P_2. While maintaining the same coupling coefficient, self-capacitance C_2 of the receiver will increase. Thus, the compensated inductance at the receiver side will decrease, making the receiver more compact and easy to be implemented in a tablet. At the receiver side, the copper plate P_4 covers nearly half of the copper plate P_3. It is noteworthy that the receiver can be placed at arbitrary location within the transmitter area. Two misalignment axes are defined in Fig. 2, i.e., Mis_X and Mis_Y. The original point is set at the top left corner.

B. Circuit Model Analysis

The circuit model of the proposed free-positioning capacitive coupler is shown in Fig. 3. Coupling capacitances exist between each pair of the plates. Because eight square plate matrixes (P_{21}, P_{22} ... and P_{28}) are in parallel to form the entire plate P_2, the coupling capacitances between P_2, and another plate are in parallel. According to Zhang *et al.* [3], there are six capacitances in the proposed vertical four-plate capacitive coupler. Therefore, among the six capacitances, the capacitances regarding plate P_2 are expressed as

$$\begin{cases} C_{12} = C_{21\_1} + C_{22\_1} + \cdots + C_{28\_1} \\ C_{23} = C_{21\_3} + C_{22\_3} + \cdots + C_{28\_3} \\ C_{24} = C_{21\_4} + C_{22\_4} + \cdots + C_{28\_4}. \end{cases} \tag{1}$$

Considering (1), Fig. 3(a) can be simplified as Fig. 3(b). Based on [3], the six-capacitance model can be transformed to the π model, as shown in Fig. 3(c). The self-capacitance C_1, C_2, and the mutual capacitance C_M are expressed as

$$\begin{cases} C_1 = C_{12} + \frac{(C_{13}+C_{14})\cdot(C_{23}+C_{24})}{C_{13}+C_{14}+C_{23}+C_{24}} \\ C_2 = C_{34} + \frac{(C_{13}+C_{23})\cdot(C_{14}+C_{24})}{C_{13}+C_{14}+C_{23}+C_{24}} \\ C_M = \frac{C_{24}C_{13}-C_{14}C_{23}}{C_{13}+C_{14}+C_{23}+C_{24}}. \end{cases} \tag{2}$$

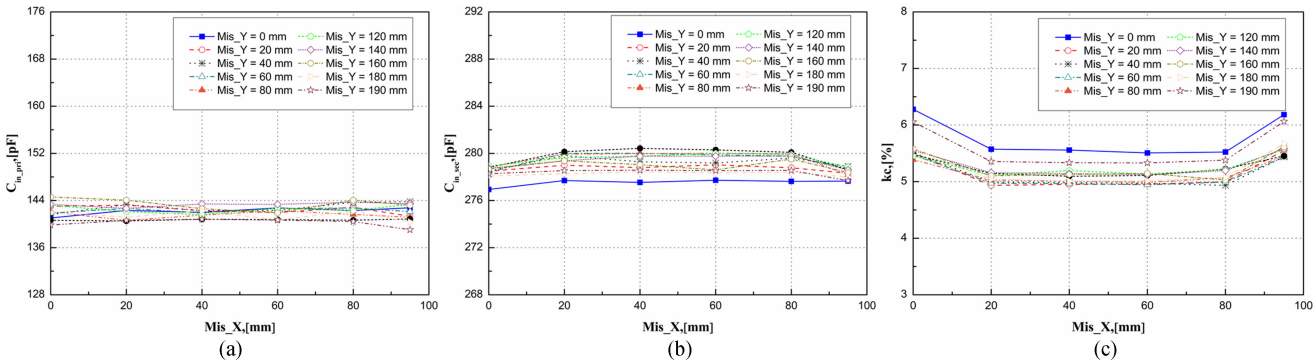

Fig. 4. (a) Coupling capacitance $C_{\text{in\_pri}}$. (b) Coupling capacitance $C_{\text{in\_sec}}$. (c) Coupling coefficient kc at different misalignment.

The coupling coefficient is defined as $k_c = C_M/\sqrt{C_1 C_2}$. The primary and secondary input capacitances are expressed as

$$\begin{cases} C_{\text{in\_pri}} = C_1 - C_M + \frac{(C_2 - C_M)C_M}{C_2} = C_1 - \frac{C_M^2}{C_2} \\ C_{\text{in\_sec}} = C_2 - C_M + \frac{(C_1 - C_M)C_M}{C_1} = C_2 - \frac{C_M^2}{C_1}. \end{cases} \tag{3}$$

C. Maxwell Simulation

All of the coupling capacitances were simulated in Maxwell software from ANSYS. With misalignment *X* and misalignment *Y* defined in Fig. 2, the variation of the coupling capacitances ($C_{\text{in\_pri}}$, $C_{\text{in\_sec}}$) and the coupling coefficient *kc* are depicted in Fig. 4. Corresponding to the experiment, 16 plexiglass (relative permittivity of 2.8) were embedded between PCB1 and PCB2 in this Maxwell simulation. It can be seen that the coupling capacitances and coupling coefficient remain stable in different misalignment conditions. The variation of $C_{\text{in\_pri}}$ is within 3.4% of the nominal value and the variation of $C_{\text{in\_sec}}$ is within 1.2%. The coupling coefficient *kc* is between 4.9% and 6.3%. Note that the compensated inductances are determined by coupling capacitances $C_{\text{in\_pri}}$ and $C_{\text{in\_sec}}$. The stabilization of the coupling capacitances indicates that the compensated inductances could remain unchanged with misalignment. Also, the coupling coefficient reflects the efficiency of the coupler, resulting in stable coil-to-coil efficiency with the variation of misalignment.

The distance between the transmitter and receiver, namely the thickness of the FR4 material in PCB2, has been studied. With the increase of the distance, the coupling capacitance $C_{\text{in\_pri}}$ will not have significant changes and the coupling coefficient *kc* will decrease. Besides, the coupling capacitance $C_{\text{in\_sec}}$ will decrease with the enhancement of the distance, leading to bigger series inductance L_2. It needs to be emphasized that at a fixed distance, for example 2.5 mm, the free-positioning feature will still be achieved. For brevity, the corresponding figures are not shown here.

With regard to the materials in the receiver case, several common materials for fabricating the PCB are selected for comparison. The comparisons are all simulated at Mis_X = 40 mm, Mis_Y = 60 mm and the corresponding simulation results are presented Table I. With the increase of the material relative permittivity, the coupling coefficient *kc* will decrease and the primary input capacitance $C_{\text{in\_pri}}$ will remain unchanged.

TABLE I
SIMULATED RESULTS FOR DIFFERENT MATERIALS IN THE RECEIVER CASE
(Mis_X = 40 mm, Mis_Y = 60 mm)

Parameters	Material in the receiver case			
	Roggers 5880	Proposed	Roggers 4350	FR4
Relative permittivity	2.2	2.6	3.66	4.4
kc	5.46%	4.96%	3.96%	3.41%
C_{in_pri}	141.6 pF	141.9 pF	144.2 pF	144.8 pF
C_{in_sec}	244.6 pF	280.0 pF	370.6 pF	432.7 pF

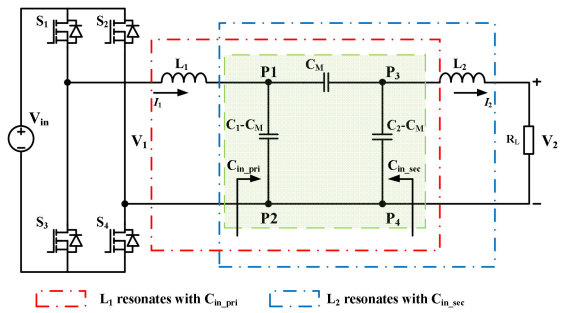

Fig. 5. Primary and secondary voltage and current waveforms.

Therefore, the relative permittivity of the material in the receiver case should not be too large. Besides, the secondary input capacitance $C_{\text{in\_sec}}$ will increase with the enhancement of the material permittivity, leading to a decrease of the series inductance L_2 inside the tablet. In our experience, the relative permittivity of the material in PCB3 should be smaller than or equal to that of the material in PCB2, which can achieve better parameters.

D. Compensation Topology of the Proposed Capacitive Coupler

Since it is intended to be applied to tablet application, compensation components should be as fewer as possible to save space and cost. Two inductances are connected in series with the coupler, resulting in a double-sided *L* compensation circuit, as shown in Fig. 5. Similar to [10], the circuit is working at a constant-current mode and it maintains unity power factor at both the primary and secondary sides. Here, it needs to be emphasized that the external parallel capacitors at both the primary and secondary sides are removed comparing with [10]. That is

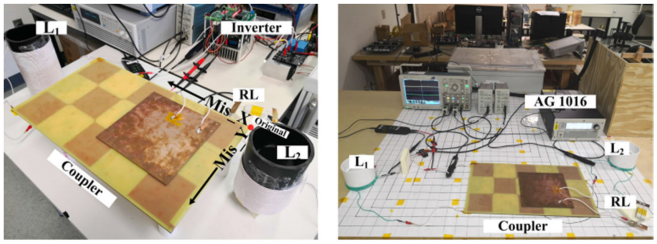

(a) (b)

Fig. 6. Fabricated prototype and experimental setup of the capacitive coupler system at (a) 1 MHz and (b) 3.45 MHz.

because the distance between P_1 and P_2, P_3 and P_4 are small and the relative permittivity of F4B is bigger than air, resulting in enough self capacitances C_{12} and C_{34}. Two series inductances L_1 and L_2 at the primary and secondary sides are resonating with $C_{\text{in\_pri}}$ and $C_{\text{in\_sec}}$, respectively. Thus, the inductances are calculated as

$$\begin{cases} L_1 = \frac{1}{\omega^2 C_{\text{in\_pri}}} = \frac{C_2}{\omega^2 (C_1 C_2 - C_M^2)} \\ L_2 = \frac{1}{\omega^2 C_{\text{in\_sec}}} = \frac{C_1}{\omega^2 \left(C_1 C_2 - C_M^2\right)}. \end{cases} \tag{4}$$

The load current I_2 and the output power are expressed as

$$I_2 = \frac{\omega(C_1 C_2 - C_M^2)V_1}{C_M}$$

$$P_{\text{out}} = \frac{\omega^2 (C_1 C_2 - C_M^2)^2 V_1^2}{{C_M}^2} R_L. \tag{5}$$

III. Experiment and Discussion

The prototype of the free-positioning capacitive coupler was fabricated and tested, as shown in Fig. 6. With structures and dimensions presented in Figs. 1 and 2, three PCBs were fabricated to integrate the capacitive coupler. Eight short copper strips of 3.5 mm width were used to connect the eight small copper plates of P_2 in parallel. Several small plexiglass were applied to fill in the air layer between PCB1 and PCB2, thus, separating them. In practical applications, this air gap layer can also be achieved by cutting small gaps on PVC tubes or wood and then insert the metal plates into these gaps [2], [3]. Another option is to drill several small holes on PCB2. Screws and nuts can be utilized to adjust the distance between PCB1 and PCB2. The ac source at 1 MHz was realized by an H-bridge inverter, consisting of Silicon carbide (SiC) MOSFETs (C2M0080120D). It is noteworthy that this SiC MOSFET is not necessary for 5 W output. In practical applications, it can be replaced by other suitable low voltage MOSFETs. As for 2.17 and 3.45 MHz resonant frequencies, the ac sources were provided by an AG 1016 from T&C Power. The load resistance R_L is chosen to be 7.25 Ω. According to the Maxwell simulation, the coupling coefficient is the lowest at the curve Mis_Y = 20 mm and Mis_Y = 60 mm. Thus, to acquire an evenly distributed efficiency with misalignment, $C_{\text{in\_pri}}$ of 144.3 pF and $C_{\text{in\_sec}}$ of 279.4 pF were measured at Mis_X = 40 mm, Mis_Y = 60 mm. Based on (4), compensated L_1 and L_2 were chosen as 175.5 μH and 90.7 μH, respectively. Since the skin depth of 1 MHz is 65 μm, the 1500-strand AWG 44 Litz-wire with a single wire diameter of 50 μm was selected for inductors to reduce ac resistance. As for higher frequencies of 2.17 and 3.45 MHz, the 1200-strand AWG 46 Litz-wire with a single wire diameter of 40 μm was selected.

As indicated in Fig. 6, we moved the receiver along axis Mis_X and Mis_Y to verify the free-positioning characteristic. Mis_X ranges from 0 to 95 mm with an increment of 20 mm. Mis_Y ranges from 0 to 195 mm with an increment of 20 mm. Since the transmitter of the coupler is a repetitive structure, the test area has already surpassed one period. The test covered 81.25% area of the whole transmitter and the test points were 66 in total. The input source voltage varied in the test process to maintain the output power to be 5 W at 1 MHz and 15 W at other two higher resonant frequencies. The range for the input voltage V_1 is 26.2 to 40.5 V at 1 MHz, 30 to 35 V at 2.17 MHz and 27 to 34 V at 3.45 MHz. It is worth noting that at 1 MHz, except for the red curve Mis_X = 0, most of the input voltages are between 30 and 36 V. Specifically, among the 55 tested points, 48 test points are between 30 and 36 V. The corresponding measured coil-to-coil efficiency with the variation of Mis_X and Mis_Y were shown in Fig. 7. Note that all of the measured efficiencies were between 52% and 56% at 1 MHz, most of the measured efficiencies were between 60% and 66% at 2.17 MHz and most of the measured efficiencies were between 52% and 58% at 3.45 MHz, which indicated that the free-positioning property had been achieved. Here, it needs to point out that few efficiency points at Mis_X = 0 mm and Mis_X = 95 mm (the edge of the capacitive coupler) are beyond these efficiency ranges because the corresponding coupling coefficients are higher than other areas in accordance with Fig. 4(c). The experimental waveform at Mis_X = 0, Mis_Y = 0 for 1 MHz resonant frequency, waveforms at Mis_X = 0, Mis_Y = 160 mm for 2.17 MHz resonant frequency and waveforms at Mis_X = 95 mm, Mis_Y = 195 mm for 3.45 MHz resonant frequency are shown in Fig. 8 and the corresponding efficiencies are 52.25%, 67.4%, and 75.12%, respectively.

For comparison purpose, several existing techniques for consumer electronics with the same output power rating are listed in Table II. It can be concluded from the table that the efficiency range of the proposed CPT system is comparable to the existing WPT techniques regarding consumer electronics. In the proposed free-positioning CPT system, since the dissipation factor *tanδ* of the material F4B is 0.0007 and that of the FR4 material is 0.02, the power loss of the system is mainly induced by FR4 dielectric layer. The planar size of the FR4 dielectric layer is relatively large and it is supposed to be integrated into the table or big pad. Therefore, the heat dissipation will not be a big issue in the proposed system. In future research, a suitable and cost-effective material is needed to replace FR4, leading to enhancement of efficiency. Inexpensive glass will be a possible material to substitute FR4 because the relative permittivity of glass is 4.6 to 5.75, which is comparable to the FR4 (4.4). Also, the dissipation factor *tanδ* of glass is 0.0006 to 0.0036, which is much lower than FR4 (0.02) [14].

Until now, few studies on multiple megahertz CPT were proposed. Thus, the experimental results at 1, 2.17, and 3.45 MHz were all presented in this letter as references. For practical

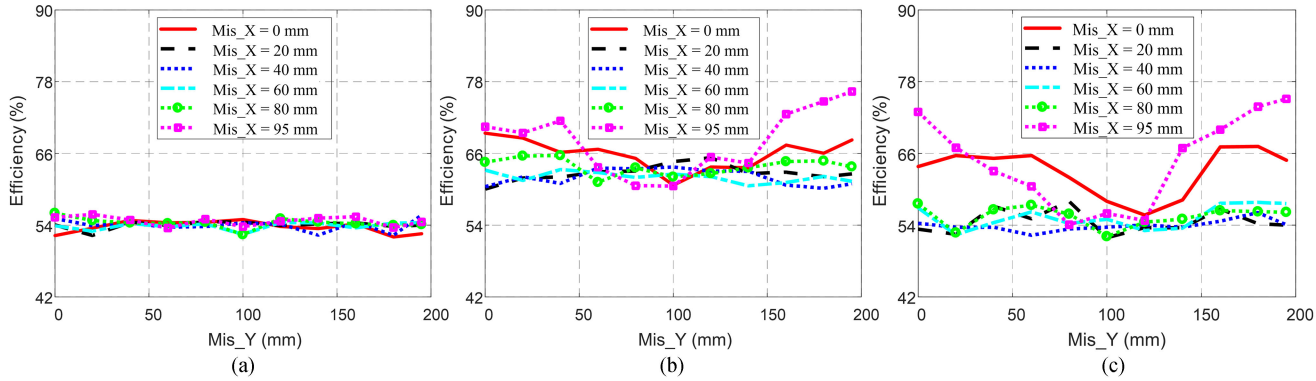

Fig. 7. Measured efficiencies of the proposed capacitive coupler at different misalignment for (a) 1MHz resonant frequency with 5 W output power, (b) 2.17 MHz resonant frequency with 15 W output power, and (c) 3.45 MHz resonant frequency with 15 W output power.

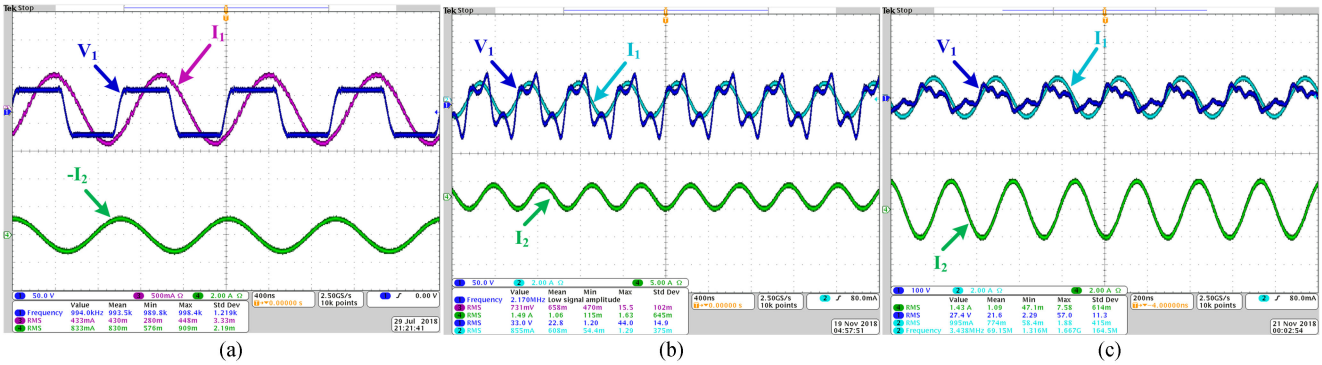

Fig. 8. Experimental waveforms at (a) Mis_X = 0, Mis_Y = 0 for 1 MHz resonant frequency, (b) Mis_X = 0, Mis_Y = 160 mm for 2.17 MHz resonant frequency, and (c) Mis_X = 95 mm, Mis_Y = 195 mm for 3.45 MHz resonant frequency.

TABLE II
COMPARISONS OF WIRELESS CHARGING SYSTEMS AT SAME OUTPUT POWER RATING FOR CONSUMER ELECTRONICS

Scheme	Output Power [W]	Efficiency [%]
Liu et al. [9]	1.6	54
Choi et al. [11]	4	16
Hu et al. [12]	10s	44.3
Liu et al. [13]	2~8	47~77
Proposed 1 MHz	5	52~56
Proposed 2.17 MHz	15	60~66
Proposed 3.45 MHz	15	52~58

consideration, the compensated inductance L_2 is supposed to be integrated into a tablet. Since the compensated inductance at 3.45 MHz is relatively small, the 3.45 MHz resonant frequency is preferred in practical. In actual industrial applications, the strand of the Litz-wire for compensated inductances at 3.45 MHz can be reduced to 400 (sufficient for 15 W output power), leading to further reduced volume of compensation inductances.

IV. CONCLUSION

In this letter, a novel capacitive coupler array with free-positioning feature was proposed for mobile tablet applications. Two repetitive PCBs of 480 mm × 290 mm were designed to construct the transmitter, which can be integrated into a small table. Another PCB of 195 mm × 195 mm was proposed to form the receiver, which can fit into a mobile tablet. Since the structures were vertically arranged and only two inductances were applied for compensation, the capacitive coupler became compact. Maxwell FEA simulation results were presented and the equivalent model was derived. While maintaining the output power at 5 W for 1 MHz, 15 W for 2.17 MHz and 3.45 MHz, all of the measured coil-to-coil efficiencies were between 52% and 56% at 1 MHz, most of the measured coil-to-coil efficiencies were between 60% and 66% at 2.17 MHz and most of the measured coil-to-coil efficiencies were between 52% and 58% at 3.45 MHz. In future research, the efficiency of the system will be increased by replacing the FR4 material.

REFERENCES

[1] J. Dai and D. Ludois, "A survey of wireless power transfer and a critical comparison of inductive and capacitive coupling for small gap applications," *IEEE Trans. Power Electron.*, vol. 30, no. 11, pp. 6017–6029, Nov. 2015.

[2] F. Lu, H. Zhang, H. Hofmann, and C. Mi, "A double-sided LCLC compensated capacitive power transfer system for electric vehicle charging," *IEEE Trans. Power Electron.*, vol. 30, no. 11, pp. 6011–6014, Nov. 2015.

[3] H. Zhang, F. Lu, H. Hofmann, W. Liu, and C. Mi, "A four-plate compact capacitive coupler design and LCL-compensated topology for capacitive power transfer in electric vehicle charging application," *IEEE Trans. Power Electron.*, vol. 31, no. 12, pp. 8541–8551, Dec. 2016.

[4] B. H. Choi, D. T. Nguyen, S. J. Yoo, J. H. Kim, and C. T. Rim, "A novel source-side monitored capacitive power transfer system for contactless mobile charger using class-E converter," in *Proc. IEEE Veh. Technol. Conf.*, 2014, pp. 1–5.

[5] D. Shmilovitz, A. Abramovitz, and I. Reichman, "Quasi-Resonant LED driver with capacitive isolation and high PF," *IEEE J. Emerg. Sel. Topics Power Electron.*, vol. 3, no. 3, pp. 633–641, Apr. 2015.

[6] R. Jegadeesan, Y. X. Guo, and M. Je, "Electric near-field coupling for wireless power transfer in biomedical applications," in *Proc. IEEE Int. Microw. Workshop Ser. Biomed. Healthcare Appl.*, 2013, pp. 1–3.

[7] C. K. Chang, G. G. Silva, A. Kumar, S. Pervaiz, and K. K. Afridi, "30 W capacitive wireless power transfer system with 5.8 pF coupling capacitance," in *Proc. IEEE Wireless Power Transfer Conf.*, pp. 1–4.

[8] S. Li, Z. Liu, L. Zhu, C. Shuai, and Z. Chen, "Wireless power transfer by electric field resonance and its application in dynamic charging," *IEEE Trans. Ind. Electron.*, vol. 63, no. 10, pp. 6602–6612, Oct. 2016.

[9] C. Liu, A. P. Hu, B. Wang and N. C. Nair, "A capacitively coupled contactless matrix charging platform with soft switched transformer control," *IEEE Trans. Ind. Electron.*, vol. 60, no. 1, pp. 249–260, Jan. 2013.

[10] F. Lu, H. Zhang, H. Hofmann and C. C. Mi, "A double-sided LC-compensation circuit for loosely coupled capacitive power transfer," *IEEE Trans. Power Electron.*, vol. 33, no. 2, pp. 1633–1643, Feb. 2018.

[11] B. H. Choi, D. T. Nguyen, S. J. Yoo, J. H. Kim, and C. T. Rim, "A novel source-side monitored capacitive power transfer system for contactless mobile charger using class-E converter," in *Proc. IEEE Veh. Technol. Conf.*, 2014, pp. 1–5.

[12] A. P. Hu, C. Liu, and H. L. Li, "A novel contactless battery charging system for soccer playing robot," in *Proc. 15th IEEE Int. Conf. Mechatronics Mach. Vis. Pract.*, Auckland, New Zealand, 2008, pp. 646–650.

[13] X. Liu and S. Y. Hui, "Optimal design of a hybrid winding structure for planar contactless battery charging platform," *IEEE Trans. Power Electron.*, vol. 23, no. 1, pp. 455–463, Jan. 2008.

[14] Dielectric Constant, Strength, & Loss Tangent. Dec. 27, 2018. [Online]. Available: http://www.rfcafe.com/references/electrical/dielectric-constants-strengths.htm. Accessed on: Dec. 27, 2018.